Robust Hybrid Supervisory Control for a 3-DOF Spacecraft in Close-Proximity Operations ⋆

Giulia Zucchini * **Bharani P. Malladi** **
Ricardo G. Sanfelice *** **Eric A. Butcher** **

* *Department of Electrical, Electronic and Information Engineering (DEI), University of Bologna, Bologna, 40136 IT (e-mail: giulia.zucchini4@studio.unibo.it)*
** *Department of Aerospace and Mechanical Engineering, University of Arizona, Tucson, AZ 85721 USA (e-mail: malladi@email.arizona.edu, ebutcher@email.arizona.edu)*
*** *Department of Computer Engineering, University of California Santa Cruz, Santa Cruz, CA 95064 USA (e-mail: ricardo@ucsc.edu)*

Abstract: In this paper we propose a hybrid control strategy to solve the problem of rendezvous, proximity operations, and docking of an autonomous spacecraft in 3D. Due to the different constraints and tasks to perform, a hybrid systems approach is implemented to solve the problem in three phases: 1) rendezvous; 2) rendezvous with smaller relative distance; 3) docking phase; and 4) docked phase; with range and angle measurements. In this approach, we implement a supervisor that robustly coordinates the individual controllers to accomplish the whole mission. We also present the designs of these individual controllers that solve the appropriate control problems for the individual phases. Numerical results for both the nominal and perturbed case validate the hybrid control strategy for the spacecraft close-proximity mission.

Keywords: Hybrid systems, Spacecraft close-proximity missions, Supervisory control, Robustness

1. INTRODUCTION

In recent years there has been an increasing necessity to control the dynamics of relative satellite motion for close-proximity missions. Often the motion between two or more satellites is modeled assuming a circular chief orbit and a deputy orbit linearized about the chief's motion. This results in the Clohessy-Wiltshire-Hill (CWH) equations Clohessy and Wiltshire (1960); Hill (1878), which is a linear time-invariant model. Such missions include both formation flying missions and rendezvous in 3-dimensional space, where guidance, closed-loop control, and navigation algorithms must be designed taking into account mission requirements and the natural orbital dynamics of the system. Feedback control solutions for such missions may involve LQR control Kluever (1999), time-varying gain control Nazari and Butcher (2016), output tracking schemes that successfully reject disturbances Lee et al. (2014), model predictive control strategies Vazquez et al. (2011); Di Cairano et al. (2012); Weiss et al. (2015) and hybrid control strategies Malladi et al. (2016).

In this paper, we extend the hybrid control strategy for rendezvous, proximity operations, and docking of an autonomous spacecraft in Malladi et al. (2016) to a 3-dimensional spacecraft modeled using the CWH equations. Similar to the strategy presented in Malladi et al. (2016), this problem consists of the following four main phases: 1) rendezvous with large relative distance; 2) rendezvous with smaller relative distance; 3) docking phase; and 4) docked phase. We consider that the range and angle measurements are available in each phase while the state constraints and the tasks to perform are different access phases. Precisely, we contribute to the problem by

- Characterizing the family of individual controllers in the 3D case and the required properties they should induce to the closed-loop system to solve the problem within each phase of operation.
- Designing a supervisor that robustly coordinates the individual controllers so as to provide a solution to the problem.
- Providing specific controller designs that appropriately solve the control problems for individual phases and validate them numerically.

The remainder of the paper is organized as follows. The notation used throughout the paper and the needed background material on hybrid controllers is presented in Section 2. The problem of interest is formalized in Section 3 and a general hybrid feedback control solution is presented in Section 4. Section 5 presents specific designs for each controller and numerical simulations for both the nominal case as well as the more general case in which we consider

⋆ Research by R. G. Sanfelice partially supported by NSF Grants no. ECS-1150306 and CNS-1544396, and by AFOSR Grant FA9550-16-1-0015. Research by E. A. Butcher and B. Malladi partially supported by NSF Grant CMMI-1657637.

the presence of noise in measurements. Due to space limitations, additional details and the proof of the main result will be published elsewhere.

2. PRELIMINARIES

2.1 Notation

The following notation and definitions are used throughout the paper. $\mathbb{R}^n$ denotes n-dimensional Euclidean space. $\mathbb{R}$ denotes the real numbers. $\mathbb{Z}$ denotes the integers. $\mathbb{R}_{\geq 0}$ denotes the nonnegative real numbers, i.e., $\mathbb{R}_{\geq 0} = [0, \infty)$. $\mathbb{N}$ denotes the natural numbers including 0, i.e., $\mathbb{N} = \{0, 1, \ldots\}$. $\mathbb{B}$ denotes the open unit ball in a Euclidean space. Given a set S, $\overline{S}$ denotes its closure. Given a vector $x \in \mathbb{R}^n$, $|x|$ denotes the Euclidean vector norm. Given a closed set $S \subset \mathbb{R}^n$ and a point $x \in \mathbb{R}^n$, $|x|_S := \inf_{y \in S} |x - y|$. Given subsets S_1, S_2, S_3 subsets of $\mathbb{R}^n$, $S_1 + S_2 + S_3 := \{x_1 + x_2 + x_3 : x_1 \in S_1, x_2 \in S_2, x_3 \in S_3\}$. The equivalent notation $[x^\top \ y^\top \ z^\top]^\top$, and (x, y, z) is used for vectors. $S_{(+)}$ denotes the set of positive definitive matrices. $\mathbf{0}$ denotes a 3×3 matrix with zeros and $\mathbf{I}$ denotes a 3×3 identity matrix.

2.2 Hybrid controllers

In this paper, we consider stabilization problems for nonlinear control systems of the form

$$\mathcal{P}: \quad \dot{\eta} = f_P(\eta, u), \quad y = h_P(\eta) \quad (\eta, u) \in C_P \times \mathcal{U}_P \quad (1)$$

where $\mathcal{U}_P \subset \mathbb{R}^{m_P}$ is a set defining the available input values, $C_P \subset \mathbb{R}^{n_P}$ is a set where the plant state $\eta \in \mathbb{R}^{n_P}$ is allowed to evolve, $f_P : C_P \times \mathcal{U}_P \to \mathbb{R}^{n_P}$ is a function defining the continuous dynamics, and $h_P : C_P \to \mathbb{R}^{n_P}$ is the output function. A hybrid controller $\mathcal{H}_c = (C_c, f_c, D_c, G_c, h_c)$ takes the form (see Goebel et al. (2012))

$$\mathcal{H}_c: \quad \begin{cases} y_c &= h_c(u_c, x_c) \\ \dot{x}_c &= f_c(u_c, x_c) \qquad (u_c, x_c) \in C_c \\ x_c^+ &\in G_c(u_c, x_c) \qquad (u_c, x_c) \in D_c \end{cases} \quad (2)$$

where $u_c \in \mathbb{R}^{m_c}$ denotes the input to the controller, $y_c \in \mathcal{Y}_c \subset \mathbb{R}^{r_c}$ denotes the controller output, $x_c \in \mathbb{R}^{n_c}$ is the controller state, the sets C_c and D_c define regions where the controller state can flow and jump, respectively, $h_c : C_c \to \mathcal{Y}_c$ defines the output of the controller and $f_c : C_c \to \mathbb{R}^{n_c}$ the flows, while $G_c : D_c \rightrightarrows \mathbb{R}^{n_c}$ is a map that defines how the controller state x_c is updated at jumps. When $\mathcal{Y}_c = \mathcal{U}_P$ and system (1) is controlled by $\mathcal{H}_c$ via the interconnection conditions $u_c = y$, and $u = y_c$, the resulting hybrid closed-loop system $\mathcal{H}_{cl}$ is given by

$$\mathcal{H}: \quad \begin{cases} \left.\begin{aligned} \dot{\eta} &= f_P(\eta, h_c(h_P(\eta), x_c)) \\ \dot{x}_c &= f_c(h_P(\eta), x_c) \end{aligned}\right\} =: F(x) \\ \qquad\qquad (\eta, x_c) \in C, \\ \left.\begin{aligned} \eta^+ &= \eta \\ x_c^+ &\in G_c(h_P(\eta), x_c) \end{aligned}\right\} =: G(x) \\ \qquad\qquad (\eta, x_c) \in D \end{cases} \quad (3)$$

where, $C := \{(\eta, x_c) : (\eta, h_c(h_P(\eta), x_c)) \in C_P \times \mathcal{U}_P, (h_P(\eta), x_c) \in C_c\}$, $D := \{(\eta, x_c) : (h_P(\eta), x_c) \in D_c\}$.

If $\mathcal{H}_c$ is such that C_c and D_c are closed, f_c and h_c are continuous, G_c is outer semicontinuous and locally bounded, and $G_c(x_c, u_c)$ is a nonempty subset of $\mathbb{R}^{n_c}$ for all $(x_c, u_c) \in D_c$, then $\mathcal{H}_c$ is said to be well-posed. Note that this interconnection is well-posed when its data satisfies the hybrid basic conditions. For more details on the definitions of hybrid time domain, hybrid arc, hybrid basic conditions, asymptotic stability and well-posedness of a hybrid system, see Goebel et al. (2012).

3. PROBLEM DESCRIPTION

We consider a model of the chaser spacecraft given by Clohessy-Wiltshire equations, namely,

$$\begin{aligned} \ddot{x} - 2n\dot{y} - 3n^2 x &= \frac{F_x}{m_c} \\ \ddot{y} + 2n\dot{x} &= \frac{F_y}{m_c} \\ \ddot{z} + n^2 z &= \frac{F_z}{m_c} \end{aligned} \quad (4)$$

where (x, y, z) and $(\dot{x}, \dot{y}, \dot{z})$ are the position and velocity of the chaser spacecraft with respect to the target spacecraft resolved into the target LVLH (local-vertical - local-horizontal) frame, respectively; F_x, F_y and F_z are the control forces in the x, y and z directions, respectively, m_c the mass of the chaser, and $n := \sqrt{\frac{\mu}{{r_o}^3}}$, where μ is the gravitational parameter of the Earth and r_o is the orbit radius of the target spacecraft. The target spacecraft is located at $(x, y, z) = (0, 0, 0)$ and has mass m_t.

The state space representation of (4) is given by:

$$\dot{\eta} = A\eta + Bu \quad (5)$$

where $\eta := [x \ y \ z \ \dot{x} \ \dot{y} \ \dot{z}]^\top \in \mathbb{R}^6$ is the state vector, $u := [F_x \ F_y \ F_z]^\top \in \mathbb{R}^3$ is the input vector, and

$$A := \begin{bmatrix} 0 & 0 & 0 & 1 & 0 & 0 \\ 0 & 0 & 0 & 0 & 1 & 0 \\ 0 & 0 & 0 & 0 & 0 & 1 \\ 3n^2 & 0 & 0 & 0 & 2n & 0 \\ 0 & 0 & 0 & -2n & 0 & 0 \\ 0 & 0 & -n^2 & 0 & 0 & 0 \end{bmatrix}, \qquad B := \frac{1}{m_c} \begin{bmatrix} \mathbf{0} \\ \mathbf{I} \end{bmatrix}$$

are the state and input matrices, respectively. The relative position between the chaser and the target is represented by $\rho(x, y, z) := \sqrt{x^2 + y^2 + z^2}$. In addition, let $\mathcal{N}^n(0, \sigma^2)$ be the set of measurable functions in an n-dimensional Euclidean space with Gaussian distribution having zero mean and variance σ^2.

With these details, the problem to solve is the following.

Problem 1: Given positive constants m_c, m_t, μ, r_o, $u_{\max}$, $\rho_{\max} > \rho_r > \rho_d$, $\overline{V}, V_{\max}$, σ_1, σ_2, σ_3, σ_4, $t_f > t_e$, $\theta \in [0, \frac{\pi}{2})$, and $(x_p, y_p, z_p) \in \mathbb{R}^3$, design a feedback controller that measures angle and range

$$y = h(\eta) + v$$

i.e.,

$$h(\eta) = \begin{bmatrix} \arctan\left(\frac{y}{x}\right) \\ \arcsin\left(\frac{z}{\rho(x, y, z)}\right) \\ \rho(x, y, z) \end{bmatrix} \quad (6)$$

where $\arctan : \mathbb{R} \to [-\pi, \pi]$, $\arcsin : \mathbb{R} \to [0, 2\pi]$ are four-quadrant inverse tangent and inverse sine, re-

spectively, $v \in \mathcal{N}(0,\sigma_n^2)$, $n \in \{1,2,3,4\}$; and assigns u such that for every initial condition $\eta_0 \in \mathcal{M}_0 := \{\eta \in \mathbb{R}^6 : \rho(x,y,z) \in [0,\rho_{\max}], \rho(\dot{x},\dot{y},\dot{z}) \in [0,\overline{V}]\}$ of the chaser with dynamics as in (5) under the constraints

- The control signal $t \mapsto u(t)$ satisfies the "maximum thrust" constraint
$$\sup_{t\geq 0} \max\{|F_x(t)|, |F_y(t)|, |F_z(t)|\} \leq u_{\max}$$
namely, for each $t \geq 0$,
$$u(t) \in \mathcal{U}_P := \{u \in \mathbb{R}^3 : \max\{|F_x|, |F_y|, |F_z|\} \leq u_{\max}\}; \quad (7)$$
- For each $\eta \in \mathcal{M}_1 := \{\eta \in \mathbb{R}^6 \ : \ \rho(x,y,z) \in [\rho_r, \infty) \ \}$, angle and range measurements are available as in (6), and $v \in \mathcal{N}(0,\sigma_1^2)$;
- For each $\eta \in \mathcal{M}_2 := \{\eta \in \mathbb{R}^6 \ : \ \rho(x,y,z) \in [\rho_d, \rho_r) \ \}$, angle and range measurements are available as in (6), and $v \in \mathcal{N}^2(0,\sigma_2^2)$;
- For each $\eta \in \mathcal{M}_3^a := \{\eta \in \mathbb{R}^6 \ : \ \rho(x,y,z) \in [0, \rho_d) \ \}$, angle and range measurements are available as in (6) and $v \in \mathcal{N}^2(0,\sigma_3^2)$; While, in addition, if $\eta \in \mathcal{M}_3^a \cap \mathcal{M}_3^b$, where $\mathcal{M}_3^b(\theta) :=$
$$\left\{\eta \in \mathbb{R}^6 : \begin{bmatrix} \sin(\theta/2) & \cos(\theta/2) & 0 \\ \sin(\theta/2) & -\cos(\theta/2) & 0 \\ \sin(\theta/2) & 0 & \cos(\theta/2) \\ \sin(\theta/2) & 0 & -\cos(\theta/2) \end{bmatrix} \begin{bmatrix} x \\ y \\ z \end{bmatrix} \leq \begin{bmatrix} 0 \\ 0 \\ 0 \\ 0 \end{bmatrix}\right\}$$
namely, the position state is in a 3-dimensional cone with aperture θ centered about the x axis, then the following constraint on closing/approaching velocity is satisfied:
$$\eta \in \mathcal{M}_3^c := \{\eta \in \mathbb{R}^6 : \ \rho(\dot{x},\dot{y},\dot{z}) \leq V_{\max} \ \}$$
where $\rho(\dot{x},\dot{y},\dot{z}) := \sqrt{\dot{x}^2+\dot{y}^2+\dot{z}^2}$.

When the chaser docks to the target (docked-phase), the chaser-target dynamics are given as in (5) with $m_c + m_t$ in place of m_c under the constraint (7) and with available position measurements relative to a partner at location (x_p, y_p, z_p). The constrained dynamics of the chaser-target are

$$\left.\begin{array}{rcl} \dot{\eta} & = & A\eta + B_R u \\ y_b & = & h_R(\eta) := h_3(\eta) \end{array}\right\} \qquad (\eta, u) \in C_R \times \mathcal{U}_P \qquad (8)$$

where

$$B_R := \frac{1}{m_c+m_t}\begin{bmatrix}\mathbf{0}\\ \mathbf{I}\end{bmatrix}, \quad C_R := \mathcal{M},$$

$$h_R(\eta) = \begin{bmatrix} \arctan\left(\dfrac{r_x(x)}{r_y(y)}\right) \\ \arcsin\left(\dfrac{r_z(z)}{\rho(r_x,r_y,r_z)}\right) \\ \rho(r_x,r_y,r_z) \end{bmatrix},$$

$r_x(x) = x - x_p$, $r_y(y) = y - y_p$, $r_z(z) = z - z_p$, $v \in \mathcal{N}^2(0,\sigma_4^2)$ and $\rho(r_x,r_y,r_z) := \sqrt{r_x(x)^2 + r_y(y)^2 + r_z(z)^2}$.

The following holds for the η-component $t \mapsto \eta(t)$ of each solution to the closed-loop system: for some $t_{2f} < t_{3f} < t_{4f}$ such that $t_{3f} \leq t_e$, $t_{4f} \leq t_f$, we have

(1) $\eta(t_{2f}) \in \mathcal{M}_3^a \cap \mathcal{M}_3^b$ and $\rho(x(t_{2f}), y(t_{2f}), z(t_{2f})) = \rho_d$; namely, the chaser reaches the cone first;
(2) $\eta(t_{3f}) \in \mathcal{M}_3^c = \{\eta \in \mathbb{R}^6 \ : \ \eta = 0 \ \}$; namely, the chaser docks on the target next, no later than t_{3f} time units;
(3) $\eta(t_{4f}) \in \mathcal{M}_4$, where $\mathcal{M}_4 := \{\eta \in \mathbb{R}^6 : (x,y,z) = (x_p,y_p,z_p), (\dot{x},\dot{y},\dot{z}) = (0,0,0)\}$; namely, the docked chaser (or chaser-target) reach the partner location no later than t_{4f} time units. △

Remark 3.1. The values of the constants m_c, m_t, μ, r_o, $u_{\max}$, and (x_p, y_p, z_p) are imposed by the vehicles and their environment. The constants $\rho_{\max}$, ρ_r, ρ_d, $\overline{V}$, $V_{\max}$, θ, t_f, and t_e are imposed by the mission and the desired performance.

4. GENERAL HYBRID FEEDBACK CONTROL STRATEGY

Following Malladi et al. (2016), we extend the algorithm that supervises multiple hybrid controllers that are designed to cope with the individual constraints and to satisfy the desired temporal properties to 3-dimensional chaser proximity mission. Similar to Malladi et al. (2016), the supervising algorithm is modeled as a hybrid system, which we denote $\mathcal{H}_s$, and is in charge of supervising the following individual hybrid controllers:

- Hybrid controller for rendezvous from distances far from target (Phase I): this controller is denoted $\mathcal{H}_{c,1}$ and its goal is to steer the chaser to a point in the interior of $\mathcal{M}$, in particular, from points in the compact set $\mathcal{M}_1 \cap \mathcal{M}_0$.
- Hybrid controller for rendezvous in close-proximity to target (Phase II): this controller is denoted $\mathcal{H}_{c,2}$ and its goal is to steer the chaser to a point in the interior of $\mathcal{X}_{los} \subset \mathcal{M}_2 \cup \mathcal{M}_3^a$, in particular, from points in $\mathcal{M}_2$.
- Hybrid controller for docking to target (Phase III): this controller is denoted $\mathcal{H}_{c,3}$ and its goal is to steer the chaser to nearby $\eta = 0$ from points in $\mathcal{M}_2 \cup \mathcal{M}_3^a$.
- Hybrid controller for relocation of target (Phase IV): this controller is denoted $\mathcal{H}_{c,4}$ and its goal is to steer the chaser-target from nearby $\mathcal{M}_3^c$ to a neighborhood of the partner position (x_p, y_p, z_p).

The operations described above are subject to the constraints stated in Problem 1. Similar to the 2-dimensional chaser close-proximity mission presented in Malladi et al. (2016), each of the hybrid controllers operates in specific regions of the state space. The tasks performed by the controllers $\mathcal{H}_{c,3}$ and $\mathcal{H}_{c,4}$ are practical, in the sense that the trajectories η are steered from and to neighborhoods of the desired sets respectively. With this problem formulation, the goals of the individual hybrid controllers are formalized next.

Due to space limitations, the formal results about the specific controllers and the supervisor will be published elsewhere.

5. SPECIFIC DESIGNS AND SIMULATIONS

5.1 An observer-based 3D LQR design of $\mathcal{H}_{c,1}$

The controller $\mathcal{H}_{c,1}$ is designed such that the inflated closed set $\mathcal{A}_1 + \delta_1 \mathbb{B} \subset \mathcal{M}$, where $\delta_1 > 0$, is finite-time attractive for the initial conditions starting from basin of attraction induced by $\mathcal{H}_{c,1}$ in η space. A controller with linear continuous-time state feedback κ_1 given by $\kappa_1(\eta) := -K_1\eta$, where $K_1 \in \mathbb{R}^{6\times 6}$, is obtained from a LQR

controller design. A saturation on the controller is implemented to satisfy the maximum thrust constraint and the resulting closed-loop hybrid system, denoted $\mathcal{H}_1 := (C_1, F_1, D_1, G_1)$, has data given by

$$F_1(\eta) = A\eta + B\kappa_1(\eta) \quad \forall \eta \in C_1 \tag{9}$$

where $C_1 := \mathbb{R}^6$, $D_1 := \emptyset$ and arbitrary G_1 (that is, no jumps).

5.2 A logic-based line-of-sight controller design of $\mathcal{H}_{c,2}$

The hybrid controller $\mathcal{H}_{c,2}$ is designed to render the inflated closed set $\mathcal{A}_2 + \delta_2\mathbb{B}$ finite-time attractive for the solution components η, η_2 starting from D_{12}. For this purpose, using the fact that initial conditions of the chaser belong to D_{12}, we exploit the ideas in Kluever (1999) (in particular, the change of coordinates), where a proportional-derivative control law that guides the chaser to dock with the target at a desired docking direction (α^*) and position (ρ^*) is proposed. We introduce a logic variable to handle the topological obstruction of stabilizing a set on a manifold. In fact, with a continuous state feedback law, there will be antipodal points to $\mathcal{A}_2$ (nearby $\alpha = 0$) from where the chaser can move either left or right to reach the desired line of sight. While, alternatively, a discontinuous controller can be designed, such a discontinuous controller would not be robust to small measurement noise as previously shown in literature Sanfelice et al. (2006). We design a logic-based hybrid controller that steers the chaser can either clockwise or counter-clockwise to take shortest route and reach a point in $\mathcal{X}_{los}^{\varepsilon\delta}$ and be robust to small perturbations. With the proposed controller, the resulting closed-loop hybrid system is denoted $\mathcal{H}_2 := (C_2, F_2, D_2, G_2)$, and has data given by

$$\begin{aligned} F_2(\eta, h) &:= \begin{bmatrix} A\eta + B\kappa_2(h\eta) \\ 0 \end{bmatrix} \quad \forall (\eta, h) \in C_2 \\ G_2(\eta, h) &:= \begin{bmatrix} \eta \\ -h \end{bmatrix} \quad \forall (\eta, h) \in D_2 \end{aligned} \tag{10}$$

where $h \in \{-1, 1\}$ is the logic state variable of the controller, $\varrho \in (0, \pi)$ is a controller parameter, $C_2 := \{(\eta, h) \in \mathbb{R}^6 \times \{-1, 1\} : h(\alpha - \alpha^*) \geq -\varrho\}$, $D_2 := \{(\eta, h) \in \mathbb{R}^6 \times \{-1, 1\} : h(\alpha - \alpha^*) \leq -\varrho\}$. The continuous-time state feedback κ_2 is given by

$$\kappa_2(\eta) := \begin{bmatrix} \kappa_2^a(\eta_a) \\ \kappa_2^b(\eta_b) \end{bmatrix}$$

where $\eta_a := (x, y, \dot{x}, \dot{y}) \in \mathbb{R}^4$ and $\eta_b := (z, \dot{z}) \in \mathbb{R}^2$. For the PD controller done on the xy system we can express

$$\kappa_2^a(\eta_a) := \begin{bmatrix} a_x \\ a_y \end{bmatrix} = \begin{bmatrix} \cos(\alpha) & -\sin(\alpha) \\ \sin(\alpha) & \cos(\alpha) \end{bmatrix} \begin{bmatrix} a_\rho \\ a_\alpha \end{bmatrix} \tag{11}$$

$$\begin{aligned} a_\rho &= u_\rho + n_\rho, \quad a_\alpha = u_\alpha + n_\alpha \\ u_\rho &= -k_1\dot{\rho}_e - k_2\rho_e, \quad u_\alpha = -\rho(k_3\dot{\alpha}_e + k_4\alpha_e) \\ n_\rho &= -[3n^2x + \dot{y}(2n + \dot{\alpha})]\cos(\alpha) + \dot{x}(2n + \dot{\alpha})\sin(\alpha) \\ n_\alpha &= [3n^2x + \dot{y}(2n + \dot{\alpha})]\sin(\alpha) + \dot{x}(2n + \dot{\alpha})\cos(\alpha) + v_\rho\dot{\alpha} \end{aligned}$$

with k_1, k_2, k_3, k_4 positive constants, $\rho_e = \rho - \rho^*$, $\alpha_e = \alpha - h\alpha^*$ [1], $\dot{\rho} = \dot{v}_\rho$, and $v_\rho = \dot{x}\cos(\alpha) + \dot{y}\sin(\alpha)$.

[1] Once again to avoid the discontinuities associated with angle calculations, we embed the angle error on a unit circle, i.e. the error calculation is performed as $\alpha_e = atan2\left(\frac{\sin(\alpha_e)}{\cos(\alpha_e)}\right)$.

This construction is obtained by changing to a coordinate system (in polar coordinates) that is fixed to the target spacecraft with its origin moving at a constant angular rate n. The resulting hybrid feedback is such that, from points in C_2 nearby $\alpha = 0$, with $\varrho \in (0, \pi)$, it steers the chaser clockwise to $-\alpha^*$ if $\alpha < \varrho$ and counter-clockwise to α^* if $\alpha > -\varrho$.
An additional LQR controller is implemented for the z component, with the state feedback given by $\kappa_2^b(\eta_b)$ and a saturation on both controllers is implemented to satisfy the maximum thrust constraint.

5.3 A uniting local and "global" design of $\mathcal{H}_{c,3}$

The hybrid controller $\mathcal{H}_{c,3}$ steers the η components of the solutions from $\mathcal{A}_2 + \delta_2\mathbb{B}$ to $\mathcal{X}_{los}^{\varepsilon}$ in finite time. This controller is designed to induce forward invariance and to satisfy the closing speed constraints for the chaser. We do this in two stages. First, a controller with output κ_3^1, thrusts the chaser towards the reference way-point $\eta_r := [x_r \ 0 \ 0 \ 0 \ 0 \ 0]^\top \in \mathcal{X}_{los}^{\varepsilon}$ (in the y axis) within T_{3a} seconds while guaranteeing forward invariance of $\mathcal{X}_{los}^{\varepsilon} \cup \mathcal{X}_{los}^{\varepsilon\delta}$. Second, a controller with output κ_3^2 implements a damping control law that guides the chaser from $\mathcal{X}_{los}^{\epsilon}$ to the inflated set $\mathcal{A}_3 + \delta_3\mathbb{B}$ within T_{3b}, along the vertical axis and slowing down the vehicle so as to satisfy the closing speed constraint. The data of the resulting hybrid closed-loop system, which is denoted $\mathcal{H}_3 := (C_3, F_3, D_3, G_3)$, is given by

$$\begin{aligned} F_3(\eta, p) &:= \begin{bmatrix} A\eta + B\kappa_3^p(\eta) \\ 0 \end{bmatrix} \quad \forall (\eta, p) \in C_3 \\ G_3(\eta, p) &:= \begin{bmatrix} \eta \\ 3 - p \end{bmatrix} \quad \forall (\eta, p) \in D_3 \end{aligned} \tag{12}$$

where $p \in \{1, 2\}$ is a logic variable the denotes the subcontroller (κ_3^1 or κ_3^2) being used, $C_3 := \cup_{p\in\{1,2\}} C_3^p \times \{p\}$, $D_3 := \cup_{p\in\{1,2\}} D_3^p \times \{p\}$. The set C_3^1 is taken to be a compact neighborhood of the reference way-point η_r that is contained in the basin of attraction of κ_3^2. The set D_3^2 is taken as a compact neighborhood of η_r such that solutions using κ_3^1 that start in D_3^2 do not reach the boundary of C_3^1. Then, we define $C_3^2 = \overline{\mathbb{R}^6 \setminus D_3^2}$ and $D_3^1 = \overline{\mathbb{R}^6 \setminus C_3^1}$.
All the controllers are tuned in a way to satisfy the maximum thrust constraint.

5.4 A 3D LQR design of $\mathcal{H}_{c,4}$

In Phase IV, the controller $\mathcal{H}_{c,4}$ has to steer the docked chaser-target from points in D_{34} to $\mathcal{M}_4 + \delta_4\mathbb{B}$, $\delta_4 > 0$, in finite time.
A controller with linear continuous-time state feedback κ_4 given by $\kappa_4(\eta) := -K_4(\eta - \eta_p)$ is designed using the LQR method. The gain K_4 is designed to satisfy the maximum thrust constraint and with this controller, the resulting closed-loop hybrid system, denoted $\mathcal{H}_4 := (C_4, F_4, D_4, G_4)$, has data given by

$$F_4(\eta) = A\eta + B_R\kappa_4(\eta) \quad \forall \eta \in C_4 \tag{13}$$

where $C_4 := \mathbb{R}^6$, $D_4 := \emptyset$ and arbitrary G_4 (that is, no jumps).

5.5 Simulation results for the nominal case

We use $n = \sqrt{\frac{\mu}{{r_o}^3}}$, $\mu = 3.986 \times 10^{14} \frac{m^3}{s^2}$, $r_o = 7100000m$, $m_c = 500Kg$ and $m_t = 2000Kg$ in the simulations. In the problem definition provided in the previous paper Malladi et al. (2016), which we also use here for this invited session, the chaser starts at a distance of no more than $\rho_{\max} = 10Km$ away from the target. Once docked, the chaser-target has to reach a relocation position with range $\rho(x, y, z) = 20Km$, which is $10Km$ away from the partner spacecraft in worst-case time of $t_f = 12hr$. In Phase I-IV both range ρ and angle α measurements are available and hence we consider that the states $\eta \in \mathbb{R}^6$ can be easily reconstructed.

With these mission parameters, simulations for the entire closed-loop system are performed for the chaser starting from $\eta \in \mathcal{M}_0 \cap \mathcal{M}_1$, which corresponds to various initial conditions in the 10Km radius with a initial velocity $\rho(\dot{x}(0,0), \dot{y}(0,0), \dot{z}(0,0)) \in [0, 0.707m/sec]$. At this step we are assuming to have all measurements known and two LQR-based controllers are implemented for the xy and z system, respectively, with the following choice of weight matrices: $Q_{1a} = 0.015 \times I_{4\times4}$, $R_{1a} = \begin{bmatrix} 20 \times 10^4 & 0 \\ 0 & 11 \times 10^4 \end{bmatrix}$, $Q_{1b} = 1.5 \times 10^{-2} \times I_{2\times2}$, and $R_{1b} = 99 \times 10^3$. The trajectories of the chaser during Phase I are shown in Figure 1, and the chaser completes the desired maneuver in this phase in $T_1 \approx 1,7hr$. Due to the interesting chaser motion,

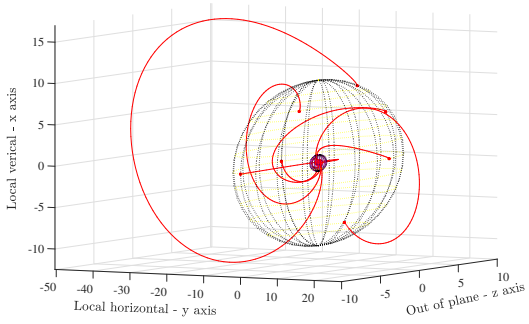

Fig. 1. Trajectories of the chaser during Phase I

we also perform multiple simulations when $\mathcal{H}_{c,2}$ is used, for initial position $(x(0,0), y(0,0), z(0,0)) \in D_{12}$, where $D_{12} := \{\eta \in \mathbb{R}^4 : \rho(x, y, z) \in [0, \rho_r]\}$, $\rho_r = 700m$, and initial velocity $\rho(\dot{x}(0,0), \dot{y}(0,0), \dot{z}(0,0)) \in [0, 0.64m/s]$. With $\rho^* = 100m$, $\alpha^* = 179deg$, and $\varrho = 10deg$, the motion of the chaser with both $h = 1$ and $h = -1$ are shown in Figure 2, which highlights the capabilities conferred by the logic variable in the hybrid controller. For the PD controller κ_{2a} the gains are chosen as: $k_1 = 40$, $k_2 = 0.1$, $k_3 = 25$, and $k_4 = 0.047$; instead, for the LQR controller, the weight matrices are: $Q = \begin{bmatrix} 138 & 0 \\ 0 & 10 \end{bmatrix}$ and $R = 30 \times 10^6$. The trajectories of the chaser during Phase II, shown in Figure 2, are completed in this phase in $T_2 \approx 1hr$. We also show the chaser evolution during the approach/closing stage (Phase III) and highlight the specific motion provided by our controller $\mathcal{H}_{c,3}$. Multiple simulations from $(x(0,0), y(0,0), z(0,0)) \in \mathcal{A}_2 + \delta_2\mathbb{B}$, where $\mathcal{A}_2 = \{\eta \in \mathbb{R}^6 : \rho = 150m, \alpha = h\,179deg\}$ and $\delta_2 = 10m$, are presented in the Figure 3. The reference way-point, where

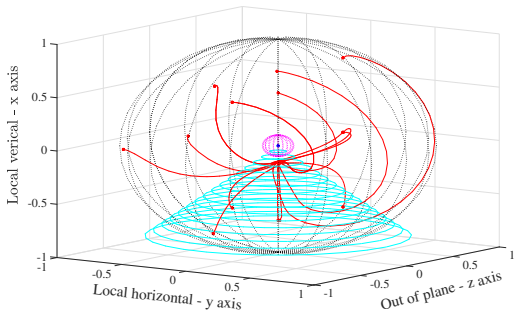

Fig. 2. Trajectories of the chaser during Phase II

the hybrid controller switches between subcontrollers is given by $\eta_r = [-25m\ 0m\ 0m\ 0m/sec\ 0m/sec\ 0m/sec]^\top$. The chaser reaches $\delta_3\mathbb{B}$ with $\delta_3 \in [2cm, 8cm]$ for several initial conditions as presented in Figure 3.
Before that switching, the controller κ_3^1 has weight matrices given by $Q_a = 38.4 \times I_{4\times4}$, $R_a = 9.7 \times 10^3 \times I_{2\times2}$, $Q_b = \begin{bmatrix} 138 & 0 \\ 0 & 10 \end{bmatrix}$, $R_b = 30 \times 10^6$ and after the switching the controller κ_3^2 has gains given by $k_1 = 0.0007$, $k_2 = 0.15$, $k_3 = 0.006$, $k_4 = 0.22$, for the xy system and $Q_b = \begin{bmatrix} 138 & 0 \\ 0 & 10 \end{bmatrix}$, $R_b = 30 \times 10^6$ as weight matrices for the z-axis LQR control. The trajectories of the chaser during Phase III are shown in Figure 3 and the chaser completes the desired maneuver in this phase in $T_3 \approx 0.8hr$.

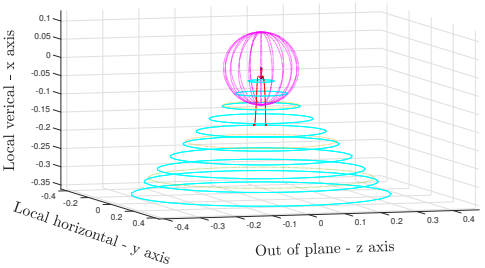

Fig. 3. Trajectories of the chaser during Phase III

In the last phase (Phase IV), the specific motion is provided by the controller $\mathcal{H}_{c,4}$ and the goal is to reach a desired partner position for the two system given by $\eta_p = [0km\ 20km\ 0km\ 0km/sec\ 0km/sec\ 0km/sec]^\top$. For that phase the 3D LQR controller has weight matrices: $Q_a = 6 \times 10^{-1} \times I_{4\times4}$, $R_a = 11 \times 10^4 \times I_{2\times2}$, $Q_b = \begin{bmatrix} 138 & 0 \\ 0 & 10 \end{bmatrix}$ and $R_b = 30 \times 10^6$. The motion of the chaser with mass $m_c + m_t$ is presented in Figure 4 and this maneuver is completed by the chaser in $T_4 \approx 1.7hr$.

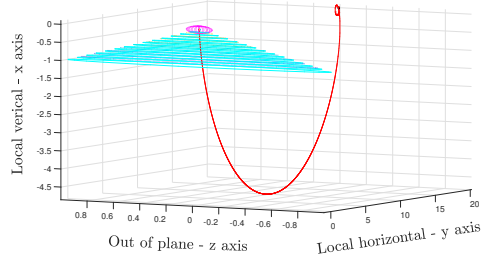

Fig. 4. Trajectories of the chaser during Phase IV

The total time constraint is satisfied: $T_1 + T_2 + T_3 + T_4 \approx 5.2hr < t_f$. An overview of the nominal motion of the chaser is given in Figure 5.

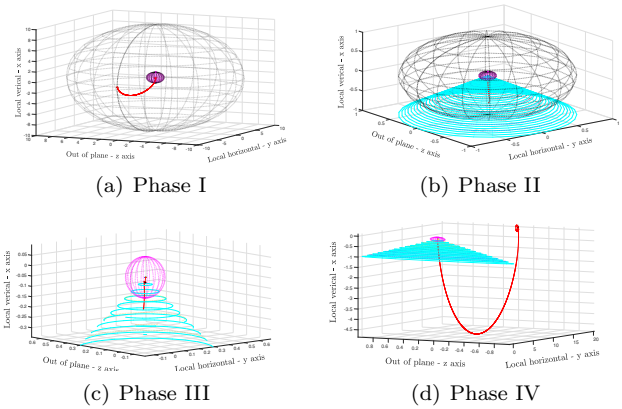

(a) Phase I (b) Phase II

(c) Phase III (d) Phase IV

Fig. 5. Overview of the nominal motion

5.6 Simulation results with noise

A more complete overview of the simulations can be done by considering noise added into the system. A small zero-mean Gaussian residual noise (considering the best performance of a chosen filter) is added to the position and velocity components in every phase. The measurement noises added to each phase are shown in Table 1.

Table 1. Variance of residual error, Phase I-IV

Phase	xy system Residual error $(\sigma_{res})^2$	z system Residual error $(\sigma_{res})^2$
I	$(\sigma_{pos})^2 = (0.5m)^2$ $(\sigma_{vel})^2 = (5 \times 10^{-5} m/sec)^2$	$(\sigma_{pos})^2 = (0.5 \times 10^{-3} m)^2$ $(\sigma_{vel})^2 = (5 \times 10^{-8} m/sec)^2$
II	$(\sigma_{pos})^2 = (0.5m)^2$ $(\sigma_{vel})^2 = (5 \times 10^{-5} m/sec)^2$	$(\sigma_{pos})^2 = (0.5 \times 10^{-3} m)^2$ $(\sigma_{vel})^2 = (5 \times 10^{-8} m/sec)^2$
III	$(\sigma_{pos})^2 = (0.5 \times 10^{-3} m)^2$ $(\sigma_{vel})^2 = (5 \times 10^{-5} m/sec)^2$	$(\sigma_{pos})^2 = (0.5 \times 10^{-7} m)^2$ $(\sigma_{vel})^2 = (5 \times 10^{-9} m/sec)^2$
IV	$(\sigma_{pos})^2 = (0.5m)^2$ $(\sigma_{vel})^2 = (5 \times 10^{-5} m/sec)^2$	$(\sigma_{pos})^2 = (0.5 \times 10^{-3} m)^2$ $(\sigma_{vel})^2 = (5 \times 10^{-8} m/sec)^2$

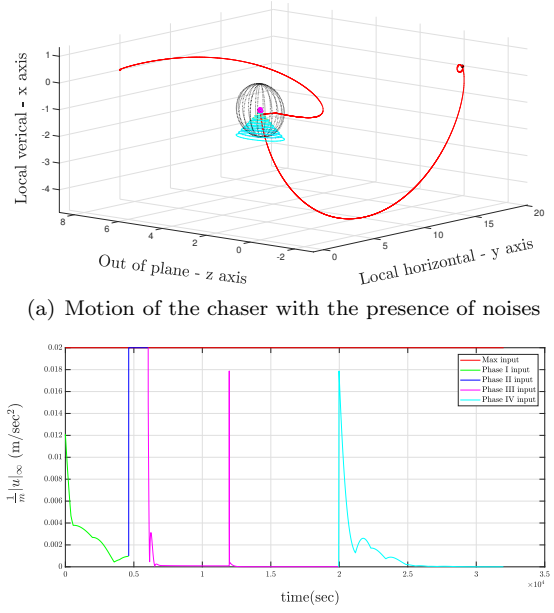

(a) Motion of the chaser with the presence of noises

(b) Input of the chaser in presence of noises

Fig. 6. Full simulation of the chaser with noise

The robustness of the controllers for small level of noise is shown in the simulations result, Figure 6, where the chaser reaches the desired neighborhood of the target while maintaining the input constraint $\|u\|_\infty \leq 0.02 m/sec^2$. The total worst case time to reach for the chaser rendezvous, docking and chaser-target rendezvous maneuver is $T_1 + T_2 + T_3 + T_4 \approx 8.88hr < t_f$, which is within specifications. [2]

6. CONCLUSION

A family of individual controllers is implemented to solve the problem of rendezvous, proximity operations and docking of an autonomous spacecraft in the 3D space. The design controllers proposed in each phase are chosen to satisfy the given constraints and the approach is validated with numerical results. Additional results on robustness of the proposed hybrid supervisory controller in presence the of measurements noise are also discussed.

REFERENCES

Clohessy, W.H. and Wiltshire, R.S. (1960). Terminal guidance system for satellite rendezvous. *Journal of the Aerospace Sciences*, 27(9), 653–658.

Di Cairano, S., Park, H., and Kolmanovsky, I. (2012). Model predictive control approach for guidance of spacecraft rendezvous and proximity maneuvering. *International Journal of Robust and Nonlinear Control*, 22(12), 1398–1427.

Goebel, R., Sanfelice, R.G., and Teel, A.R. (2012). *Hybrid Dynamical Systems: Modeling, Stability, and Robustness*. Princeton University Press, New Jersey.

Hill, G. (1878). Researches in the lunar theory. *American Journal of Mathematics*, 1, 5–26.

Kluever, C.A. (1999). Feedback control for spacecraft rendezvous and docking. *Journal of Guidance, Control, and Dynamics*, 22(4), 609–611.

Lee, D., Bang, H., Butcher, E.A., and Sanyal, A.K. (2014). Nonlinear output tracking and disturbance rejection for autonomous close range rendezvous and docking of spacecraft. *Transactions of the Japan Society for Aeronautical and Space Sciences*, 57, 225–237.

Malladi, B.P., Sanfelice, R.G., Butcher, E., and Wang, J. (2016). Robust hybrid supervisory control for rendezvous and docking of a spacecraft. In *Proceedings of the Conference on Decision and Control*, 3325 – 3330.

Nazari, M. and Butcher, E.A. (2016). Fuel efficient periodic gain control strategies for spacecraft relative motion in elliptic chief orbits. *International Journal of Dynamics and Control*, 4, 104–122.

Sanfelice, R.G., Messina, M.J., Tuna, S.E., and Teel, A.R. (2006). Robust hybrid controllers for continuous-time systems with applications to obstacle avoidance and regulation to disconnected set of points. In *Proc. 25th American Control Conference*, 3352–3357.

Vazquez, R., Gavilan, F., and Camacho, E.F. (2011). Trajectory planning for spacecraft rendezvous with on/off thrusters. *IFAC Proceedings Volumes*, 44(1), 8473–8478.

Weiss, A., Baldwin, M., Erwin, R.S., and Kolmanovsky, I. (2015). Model predictive control for spacecraft rendezvous and docking: Strategies for handling constraints and case studies. *IEEE Transactions on Control Systems Technology*, 23(4), 1638–1647.

[2] Simulation files available at: `https://github.com/HybridSystemsLab/HybridRendezvousAndDocking3DOF`